

SmartCT – Development of AI based methods for automation of RoboCT scan procedures

Frank Sukowski¹, Daniel Rauch¹, Richard Schielein¹, Tobias Schön¹, Adrian Waldyra¹, Mara Fries¹, Andreas Maier², Linda-Sophie Schneider², Gabriel Herl³, Simon Wittl³, Simon Zabler³, Sebastian Zeitel⁴, Joshua Bissels⁵, Christian Becker⁶

¹Fraunhofer Institute for Integrated Circuits IIS, Am Wolfsmantel 33, 91058 Erlangen, Germany

²Pattern Recognition Lab, University of Erlangen-Nuremberg, Martensstraße 3, 91058 Erlangen, Germany

³Technology Campus Plattling, Deggendorf Institute of Technology, Dieter-Görlitz-Platz 2, 94469 Deggendorf, Germany

⁴Max-Streicher GmbH & Co. KG, Schwaigerbreite 17, 94469 Deggendorf, Germany

⁵Pinter Guss GmbH, Brunnwiesenstraße 2, 94469 Deggendorf, Germany

⁶Becker Carbon GmbH, Fritz-Schäffer-Straße 50, 94560 Offenberg/Neuhausen, Germany

Abstract

The SmartCT system consists of AI based methods that assist users of robot-based CT systems (RoboCT) to digitalize industrial parts of almost arbitrary size and geometrical complexity with a high degree of automation. Due to the high number of degrees of freedom and thus complexity, RoboCT scan procedures are difficult to parametrize with respect to collision safety and image quality. The SmartCT assist functions help users to perform measurements quickly and safely while using advanced algorithms for geometrical image correction and 3D-CT volume reconstruction.

Keywords: CT, calibration, reconstruction, scan planning, trajectories, optimization, RoboCT, Twin Robotic CT, deep learning

1 Motivation for RoboCT

Industrial X-ray CT machines typically adopt two configurations: one with a turntable positioned between the X-ray source and the detector, and the other with a gantry that encompasses both components, rotating around the object. In both configurations, the maximum size of the inspected part is constrained by the distance between the X-ray source and the detector, as the part must be rotated to obtain projections from all viewing angles. With robot-based CT systems, this limitation is overcome by using two cooperative robots carrying the X-ray components, being able to move them on arbitrary trajectories around parts of almost arbitrary size and geometric complexity (e.g. Figure 1). The high number of degrees of freedom on the other hand makes parametrization of scan procedures very complex. One major concern is avoiding collisions between the robots with the part. But an even more important aspect is using the available degrees of freedom to optimize scan acquisition and thus CT results, depending on the shape and material of the object in question. SmartCT provides a solution using AI based algorithms that assist users in performing CT scans from the parametrization of scan procedures to the final reconstructed CT volume.



Figure 1: Examination of A-pillar on a complete car



2 Workflow

The SmartCT systems leads users from the initial part positioning to the complete 3D-CT reconstruction. The workflow is outlined in the following diagram (Figure 2). During several steps the user simply has to physically place the part into the RoboCT system, optionally load the CAD data to the SmartCT system and define the region-of-interest (ROI) to be inspected and some information about the inspection task (pore detection / surface extraction, target voxel resolution).

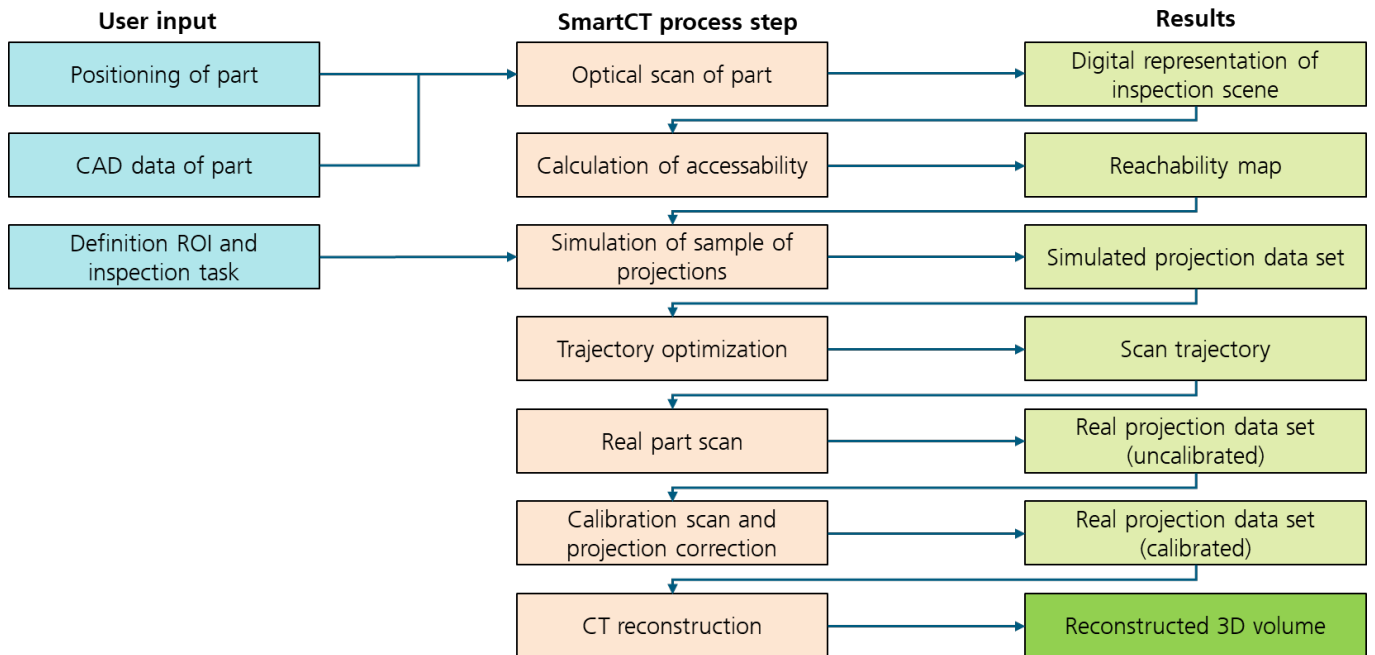


Figure 2: SmartCT workflow

2.1 Part positioning and tracking

Choosing the right scan strategy for large and complex shaped parts in terms of best imaging quality while using as little projections as possible is a trying endeavor and thus requires a multi-step workflow to be successfully realized. As first step and before any optimization strategy can calculate an appropriate scan trajectory, the system must know the shape and placement of the part to be inspected. Additionally, the measuring scene has to be analyzed for possible collision objects, like the part itself and mounting accessories, to deduce a collision-free path for the robots. To get this information in a quick and efficient way, it was chosen to introduce additional digitization modalities with a corresponding data processing pipeline to the system. Specifically, a time-of-flight-based scanner, specialized evaluation software and a digitization routine were integrated into the workflow, which are described in the next section.

After the part is positioned and securely mounted into the RoboCT machine by an expert, the complete measuring scene is digitized with a 360-degree optical time-of-flight scanner multiple times which after on-scanner scan-to-scan registration yields a surface point cloud representation of the scene. The resulting point cloud must be registered to a known coordinate system, which can be either done by manually selecting reference planes and objects in the dataset or by an automatic reference marker-based approach. Now that the scan data is in the correct frame of reference, it is cropped to a user defined active working area, resampled, and cleaned of statistical outliers. With that preprocessing as baseline, the collision mesh for use with the digital twin of the RoboCT system can be extracted by computing a convex hull around the dataset and adding an 10-20% offset along the mesh normals for extra clearance. If a more detailed collision mesh is required, alternatively a different meshing approach can be chosen, with the Alpha shapes surface reconstruction [1] as recommendation due to it delivering good enough results for collision detection while being robust to noise and tolerant regarding incomplete data.

From this point on the system can be fully operated without the risk of collision, but the part transformation in the reference coordinate system is still unknown. To obtain this transformation, it is necessary to segment the scan data representing the part from the overall scan, which also includes the structures used for mounting or holding the part. Currently a semi-manual method is used, which relies on CAD data, or a master scan to mask the relevant data. The mask has to be aligned manually, which – depending on the dataset – can be tedious. Thus, in the future an AI-supported method relying on a Self-positioning Point-based Transformer [2] implementation is set up. The segmented data can be input into a registration pipeline for fitting to a reference object, again comprising of either CAD data or a pre-scanned master scan of the part. The registration is initially tried globally via Open3Ds Fast Point Feature Histograms (FPFH) implementation [3] [4]; if the residuals are too above a certain threshold the pipeline falls back to a manual N-point based registration method, where corresponding points are picked manually. To refine

the global registration, locally Iterative Closest Point (ICP) is used, which then yields the final part transformation used for optimizing scan trajectories.

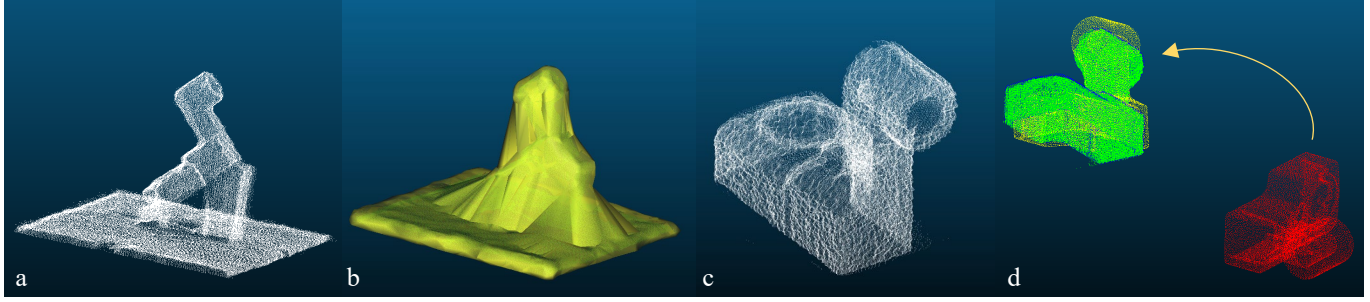


Figure 3: Pipeline steps visualized - from left to right: raw scan data of active region (a), collision object with additional offset (b), segmented part (c), registration result (d; CAD: red; target: green; global registration result: yellow; final registration result: blue)

2.2 Reachability

A highly flexible machine such as a CT device based on twin robots need a digital twin to avoid the danger of collisions between machine components and the scan object or other objects in the work volume. The digital twin of the RoboCT get the collision object, from the part positioning and tracking task, as input to avoid collisions of the robots with the scan object. The reachability calculation task get as input the scan center, the target resolution, and the focus-detector-distance. The scan center is determined from the ROI (region of interest) in object coordinates and the transformation of the object to the world coordinates from the part tracking task. The first step is to sample a set of all interesting scan poses that are possible for the task. In this case a random sphere of CT scan poses is calculated with the given target resolution, and focus-detector-distance around the scan center point. The second step is to check all the sampled poses by the digital twin if the robots can reach them without collision. That a scan pose is reachable both the detector and the source robot must be possible to reach their position without a collision to the scan object or a part of the robot system. The result of reachable scan poses is the reachability map output. The reachability map is used in the further steps that only valid robot positions are chosen.

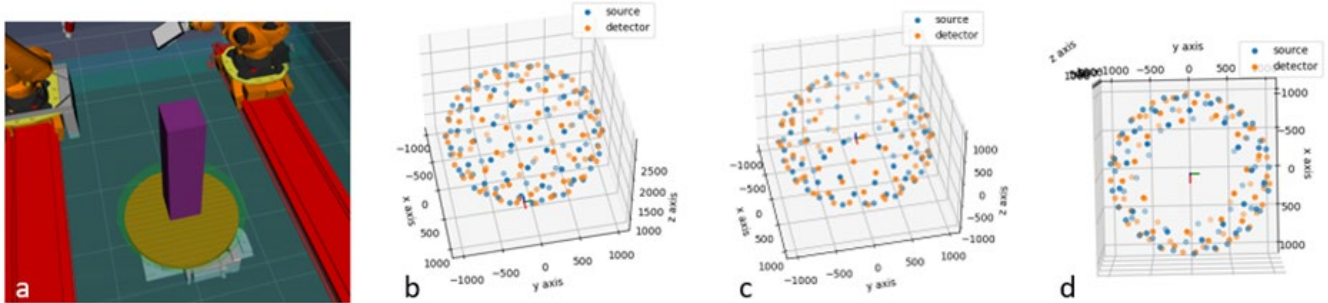


Figure 4: Reachability calculation steps: digital twin with inserted collision object (a); random pose sphere around scan center (b); reachable scan poses (c); reachable scan poses top view (d)

2.3 Projection simulation

In order to evaluate the information content and the suitability of X-ray projections for a high-quality CT scan, projections of the inspected part are simulated from a number of different viewing angles according to the reachability map. The number of projections and thus the sampling rate is chosen by the user. The generation of these virtual projections is done using the XSimulation tool [5]. The simulation works using raytracing methods from the point of origin of the emitted X-rays (focal spot of X-ray source) through the CAD model of the inspected part to each detector pixel. For the part modeling, the elemental composition and mass density has manually to be parametrized. The simulation uses realistic X-ray spectra, and each ray is attenuated by Lambert-Beer's Law. XSimulation supports user defined focal spot sizes. In that case, the points of origin of the emitted X-rays are sampled according to the spatial intensity distribution of the focal spot. The simulation can be calibrated to the real imaging system regarding system spectrum and detector blurring. The latter effect is calculated as a post-processing step after the projection was simulated. Physical effects of higher order such as the impact of X-ray scattering on the image can also be simulated, but the calculation time significantly increases.

Without scattering, the simulation time varies between some milliseconds up to one second per projection on a modern GPU depending mainly on the number of detector pixels and the focal spot subsampling rate.

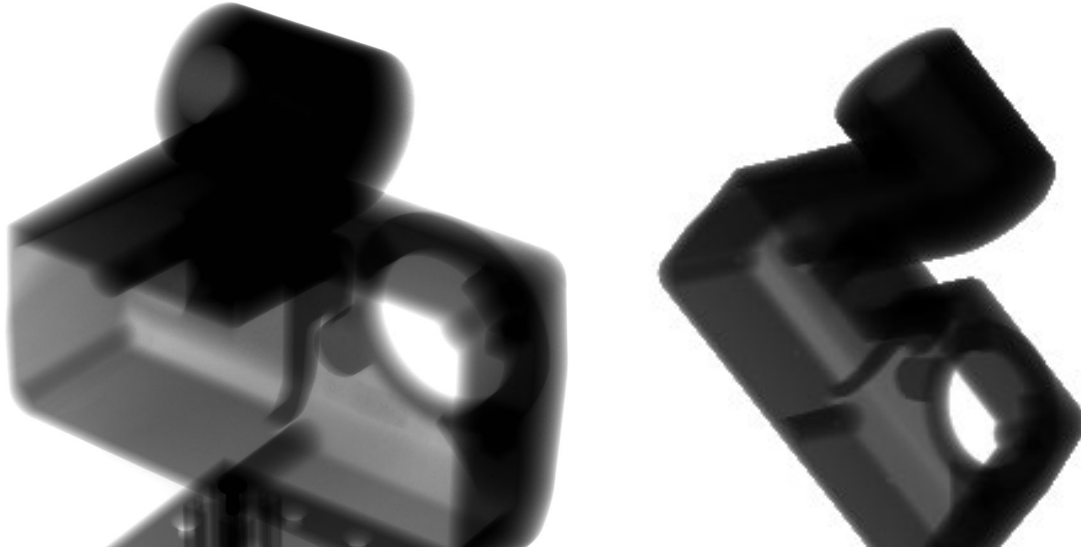


Figure 5: Real projection (left) and simulation (right) of the same industrial part

2.4 Scan trajectory optimization

Optimization of the computed tomography (CT) trajectory is an important prerequisite for exploiting the unique flexibility of the RoboCT system. For this reason, we have developed an end-to-end methodology to automate the selection of projections [6]. Our approach emphasizes identifying the most suitable projections for image reconstruction in CT imaging.

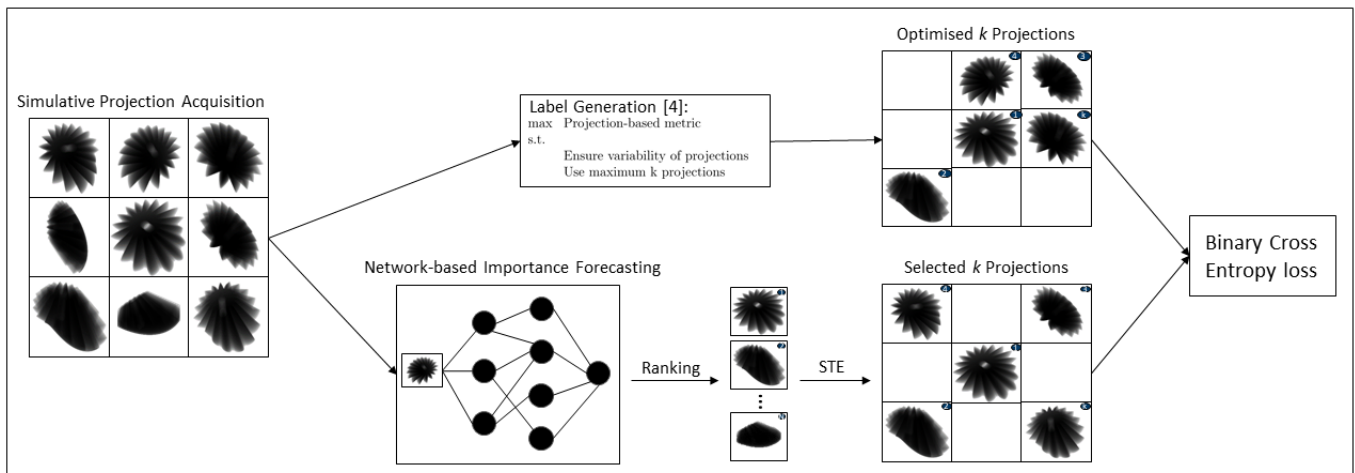


Figure 6: Overview of the training of the proposed approach. First, each projection is regressed to a single value. This value is used as a basis for the ranking. To generate a selection out of the ranking, we utilize a straight trough estimator. Binary Cross Entropy is utilized as loss function.

Our method builds upon earlier research that employed a neural network framework to acquire a projection-dependent detectability index for CT trajectory optimization [7]. However, these prior methods exhibited certain limitations, particularly in terms of ensuring dataset diversity and frequently excluded projections potentially being highly valuable. In addressing these challenges, our work introduced a three-step neural network approach in [6]. The first step involves the transformation of each projection into a singular value via a modified ResNet-18 architecture, effectively constructing a vector that characterizes the merit of each projection. This neural network attempts to imitate the behavior of projection-dependent detectability index metrics, which assess the quality of individual projections and their contributions to signal observability in the reconstructed image [8]. The second step employs a differentiable ranking operator [9] on this vector, yielding a ranking of the projections. This differentiable ranking operator reformulates the typically non-differentiable process of ranking in descending order as a linear program over the permutahedron. This allows us to seamlessly integrate this operation into our neural network framework. Finally, a Straight-Through Estimator (STE) [10] is employed to transform this ranking into a binary vector indicating the

selection of projections. This binary vector enables the network to perform backpropagation through the chosen projections during the training process. A visual representation of these essential steps is presented in Figure 5.

To effectively train our architecture for CT trajectory planning, we require a dataset of test specimens from the same object class as the target specimen. In [6], we utilized 15 Computer-Aided Design (CAD) files for training and validation. Additionally, we need information regarding reasonable Regions of Interest (ROIs) within the specimens. For each of these ROIs, we introduce an artificial defect randomly within the ROI. The labelling of our training and validation sets includes the calculation of the projection-dependent detectability index, a time-consuming task that assesses whether the inserted defect is detectable in the corresponding projection. To extend this projection-based metric to a set-based metric, we incorporate the distribution of the selected set as a figure of merit. This figure of merit can take the form of the Haversine Distance Constraint [7] or a Tuy-based data completeness metric [11]. The application of an integer program introduced in [7] provides us with the required labels. During the training and validation phases, we employ Binary Cross Entropy as our loss function. For our test dataset, we evaluate the efficacy of our approach in the domain of image reconstruction, utilizing the Structural Similarity Index (SSIM) and the Root Mean Squared Error (RMSE) as metrics to assess image quality.

2.5 Geometric calibration

Industrial robots' absolute positioning accuracy is in the most cases not precise enough for CT reconstruction. As a result, nominal robot positions are not sufficient for the reconstruction of RoboCT data. Precise geometrical information, such as projection geometries, is required to perform reconstruction an example is shown in Figure 5. For each scan position of the robots, the projection geometries must be corrected. To achieve this, we use the Direct Linear Transformation (DLT) [12]. The DLT calculates the projection geometries for each scan position using a known calibration body. A 3D printed plastic calibration body is used for this purpose. The surface of the body has steel balls arranged in helical form. The position of the steel balls, which is measured prior to using a metrological CT system, is an input to the DLT algorithm. When a new robot trajectory is generated, all scan positions are calibrated using the DLT algorithm and the designed calibration body. The high repeatability of the robots guarantees accurate repetitions of the robot trajectory with the object.

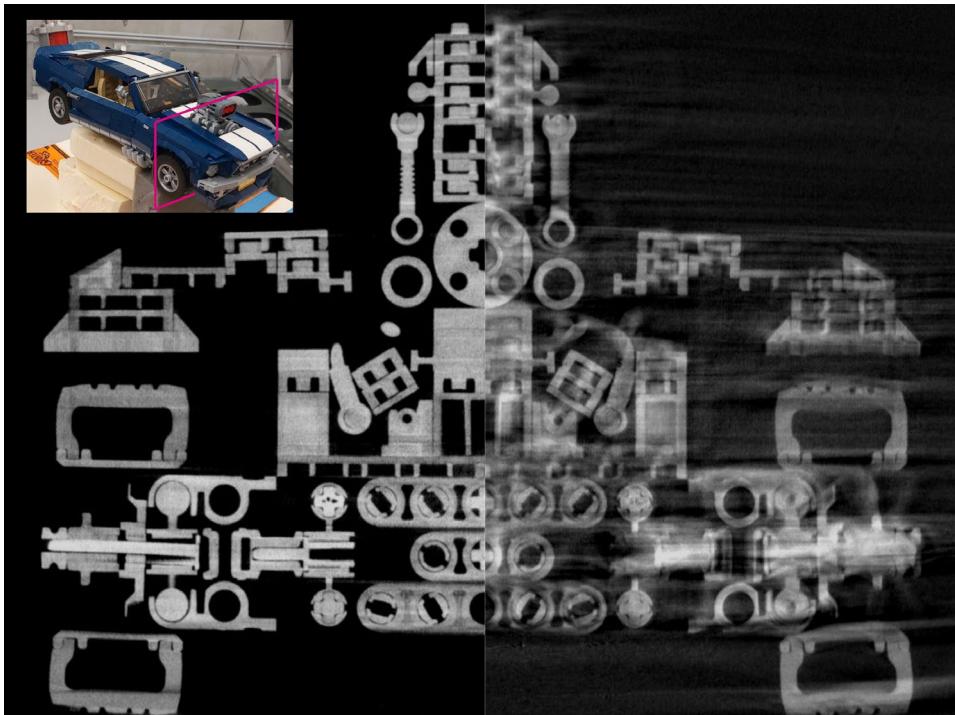


Figure 7: Influence of geometric errors on reconstruction: The figure shows a single slice of a reconstructed Mustang Lego model, with the reconstructed slice shown as a pink rectangle in the upper left corner of the inserted image. The reconstruction slice is split so that the left-hand side shows the corrected projection geometry, and the right-hand side shows the same slice with the uncorrected projection geometry.

A decisive prerequisite for the application of the DLT algorithm is the exact assignment of steel spheres, which are represented as ellipses in X-ray projections, to their corresponding counterparts in the calibration body. In our project, we solved this mapping problem with the help of an AI model [13]. The decisive advantage of this AI approach is that it allows a freely selectable arrangement of the spherical elements in the calibration space. In contrast to conventional methods, this AI approach allows the user to configure the spatial arrangement themselves, as shown in Figure 4. The configuration used ensures a uniform distribution of the spheres over the entire calibration body, regardless of the projection angle. This spatial arrangement contributes significantly to improving the calibration accuracy.

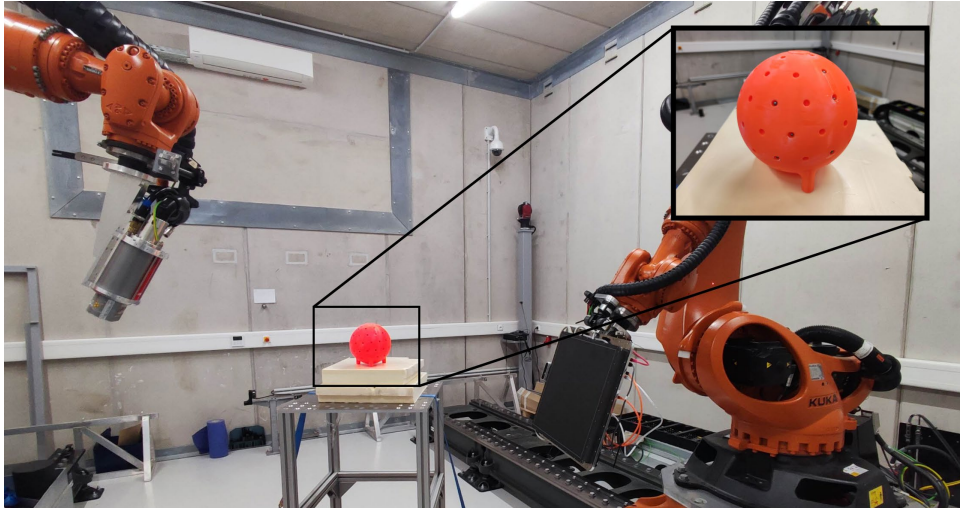


Figure 8: Calibration setup at RoboCT system at the Deggendorf Institute of Technology.

2.6 Algebraic CT reconstruction

In contrast to analytical reconstruction techniques, which are commonly used for standard circular trajectories, iterative algebraic reconstruction methods can reconstruct arbitrary scan trajectories and are therefore the main choice for flexible systems such as RoboCT. Our reconstruction algorithms are based on the simultaneous algebraic reconstruction technique (SART), a variant that in terms of implementation can be described as an algorithm with three basic steps (see Figure 9): for each trajectory point, compute a virtual projection of the current volume (forward-projection), compare the computed projection with the corresponding measured projection (correction) and correct the volume respectively (back-projection) [14]. These steps are commonly computed on the GPU due to considerable runtime gains, where the volume is stored in GPU-memory using float. Since the forward-projection step requires the entire volume, the GPU-memory quickly reaches its limits with modern applications and RoboCT in particular; a 2048x2048x2048 volume, for example, already corresponds to 32GB in the GPU-memory. We modified the SART in this respect, and further extended it for the use on multi-GPU systems, resulting in two algorithms that can be used for reconstruction.

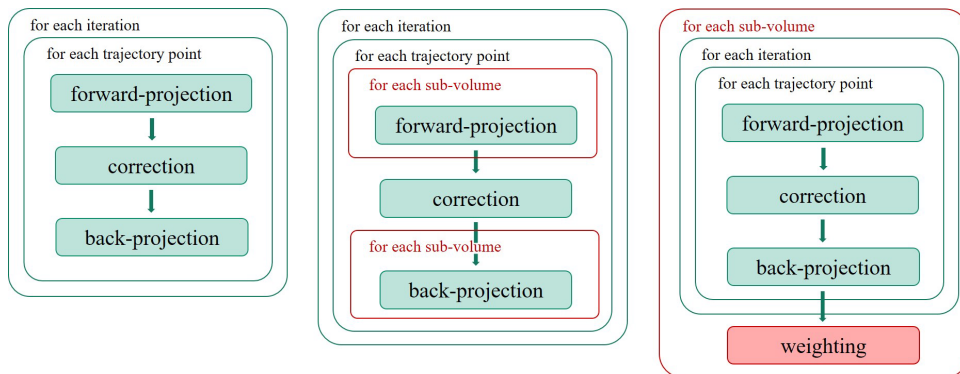


Figure 9: Reconstruction algorithm visualized - from left to right: original SART, precise reconstruction method, approximate reconstruction method

In a modification for precise reconstruction, we utilize the fact that the forward-projection, just like the back-projection, is a commutative operation. The volume is therefore split into disjoint sub-volumes, and for each trajectory point, the sub-volumes are copied group-wise into GPU-memory, performing multiple forward-projections and sequentially summing up their results. The back-projection is performed on the sub-volume groups in a similar manner (see Figure 9). Additional automatically selected adjustments allow the use of double buffering to minimize idle times, or the option to keep the volume in GPU-memory if it can fit entirely, which makes the reconstruction process identical to the original SART. Overall, this precise reconstruction method results in reconstructed volumes almost identical to those of the original SART but requires a large number of copy operations.

To reduce the number of copy operations, we introduced a second, approximate reconstruction method in which we perform the forward- and back-projection directly on each sub-volume group. This leads to artifacts due to the forward-projection of an incomplete volume. There are mainly two reasons for this: the influence of the missing volume is ignored in the virtual projection

as well as in the computation of ray lengths used for the normalization of the correction values. This leads to higher correction values due to the discrepancy between computed and measured projection, which are then incorporated more strongly into the volume due to the reduced normalization of the values. Depending on the trajectory, the resulting artefacts mostly occur at the edges of the sub-volumes, where the missing volume has the most impact. We now add additional sub-volumes at the block transitions of the previous sub-volumes to cover the artefacts with the middle part of the additional sub-volumes (and vice versa). The original SART algorithm is applied group-wise to all sub-volumes and the resulting reconstruction assembled in a weighted manner (see Figure 9). Since this only addresses the already occurring artefacts, we added two modifications regarding their origin. The first modification allows the computation of the ray lengths considering the entire volume, correcting the normalization of the correction values. For the second modification, the influence of previously forward-projected sub-volume groups is weakened by subtracting their computed projections from the measured projections. These modified measured projections will then be used for the comparison of subsequent sub-volume groups, reducing the discrepancy between measured and computed projection.

Regarding the runtime, despite reconstructing parts of the volume twice, the approximate method is generally faster than the precise method. The decision as to whether the approximate reconstruction method is sufficient, possibly with either or both modifications, is entirely component- and task-specific. Figure 10 shows the result of the three reconstruction methods on a simulated RoboCT data set.

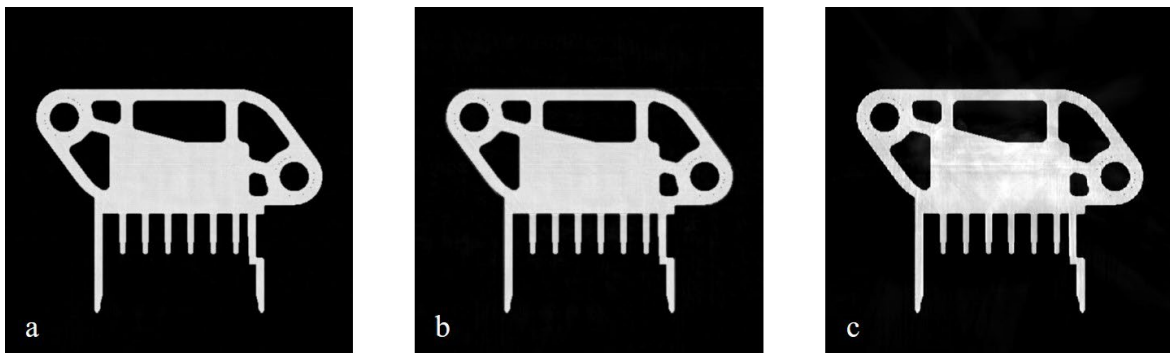


Figure 10: Results of different reconstruction methods - from left to right: original SART (a), precise reconstruction method (b), approximate reconstruction methods with both modifications (c)

3 Conclusion

With SmartCT, an integral system is developed assisting RoboCT users from the part placement over choice of trajectory till the complete reconstructed volume with AI based methods. With SmartCT, the operation of such systems becomes faster, safer and the results better in terms of image quality. Testing labs as well as the production industry of large parts, e. g. integral car body manufacturers like Giga-casting plants benefits from that technology since SmartCT enables the usage of RoboCT systems outside scientific laboratories.

References

- [1] H. Edelsbrunner, D. G. Kirkpatrick and R. Seidel: “On the shape of a set of points in the plane”, *IEEE Transactions on Information Theory*, 29 (4): 551–559, 1983
- [2] Jinyoung Park, Sanghyeok Lee, Sihyeon Kim, Yunyang Xiong, Hyunwoo J. Kim, “Self-positioning Point-based Transformer for Point Cloud Understanding”, 2023
- [3] Qian-Yi Zhou, Jaesik Park and Vladlen Koltun, “Open3D: A Modern Library for 3D Data Processing”, *arXiv:1801.09847*, 2018
- [4] R. Rusu, N. Blodow, and M. Beetz, “Fast Point Feature Histograms (FPFH) for 3D registration”, *ICRA*, 2009.
- [5] R. Schielein, “Analytische Simulation und Aufnahmeplanung für die industrielle Röntgencomputertomographie”, *doctoral thesis, University of Würzburg*, 2018
- [6] L.-S. Schneider, M. Thies, C. Syben, R. Schielein, M. Unberath, A. Maier, “Task-based Generation of Optimized Projection Sets using Differentiable Ranking”, *Fully3D New York*, 2023, *arXiv preprint: 2303.11724*
- [7] L.-S. Schneider, M. Thies, R. Schielein, C. Syben, M. Unberath, A. Maier, “Learning-based Trajectory Optimization for a Twin Robotic CT System”, *12th Conference on Industrial Computed Tomography (iCT) 2023 (Fürth, February 27, 2023 - March 2, 2023)*, *NDT.net Issue: 2023-03 2023*, DOI: 10.58286/27748
- [8] G. J. Gang, J. W. Stayman, W. Zbijewski, et al. “Task-based detectability in CT image reconstruction by filtered backprojection and penalized likelihood estimation”, *Medical Physics* 41.8 (Aug. 2014), p. 081902. DOI: 10.1118/1.4883816.
- [9] M. Blondel, O. Teboul, Q. Berthet, et al., “Fast Differentiable Sorting and Ranking”, 2020, DOI: 10.48550/ARXIV.2002.08871.
- [10] Y. Bengio, N. Léonard and A. C. Courville, “Estimating or Propagating Gradients Through Stochastic Neurons for Conditional Computation”, *CoRR abs/1308.3432* (2013).
- [11] G. Herl, J. Hiller, A. Maier, “Scanning trajectory optimisation using a quantitative Tuybased local quality estimation for robot-based X-ray computed tomography”, *Nondestructive Testing and Evaluation*, 35 (2020) 287-303
- [12] Hartley, R.; Zisserman, A., “Multiple View Geometry in Computer Vision”, *Cambridge University Press*, 2011
- [13] S. Wittl, A. Weiss, G. Herl, S. Zabler (2023), „Keep Attention to the Mapping: Application of AI for Geometric X-Ray CT Scan Calibration”, *12th International Conference on Industrial Computed Tomography (iCT2023)*, Fürth
- [14] A. H. Andersen and C. K. Avinash, “Simultaneous algebraic reconstruction technique (SART): a superior implementation of the ART algorithm”, *Ultrasonic imaging* 6.1 (1984): 81-94.